

# Properties of rapamycin solid lipid nanoparticles for lymphatic access through the lungs – part II: the effect of nanoparticle charge

Emelie Landh<sup>1,2</sup>, Lyn M Moir<sup>1,2</sup>, Daniela Traini<sup>1,2</sup>, Paul M Young<sup>1,2</sup> & Hui X Ong<sup>\*,1,2</sup>

<sup>1</sup>Respiratory Technology, Woolcock Institute of Medical Research, Glebe, NSW, 2037, Australia

<sup>2</sup>Discipline of Pharmacology, Faculty of Medicine & Health, Sydney, NSW, 2006, Australia

\*Author for correspondence: Tel.: +61 2 91140373; [ong.hui@sydney.edu.au](mailto:ong.hui@sydney.edu.au)

**Aim:** Lymphangioliomyomatosis is characterized by smooth muscle-like cells in the lungs that spread to other organs via lymphatic vessels. Oral rapamycin is restricted by low bioavailability approximately 15%. The aim of the present study is to systematically investigate the effect of inhaled rapamycin solid lipid nanoparticles (Rapa-SLN) surface charge on efficacy and penetration into the lymphatics. **Materials & methods:** Rapa-SLN formulations with different charge: neutral, positive and negative, were produced and assessed for their physicochemical particle characteristics and efficacy *in vitro*. **Results:** Negative Rapa-SLNs were significantly faster at entering the lymphatic endothelium and more potent at inhibiting lymphangiogenesis compared with neutral and positive Rapa-SLNs. **Conclusion:** Negative Rapa-SLNs showed efficient lymphatic access and should therefore be investigated further as a treatment for targeting extrapulmonary lymphangioliomyomatosis.

First draft submitted: 4 May 2020; Accepted for publication: 11 June 2020; Published online: 19 August 2020

**Keywords:** inhalation • lymphangioliomyomatosis • lymphatic system • rapamycin • solid lipid nanoparticles • surface charge

Lymphangioliomyomatosis (LAM) is a lung disease that results from a mutational inactivation of the tuberous-suppressor genes, tuberous sclerosis complex 1 and 2 (TSC1/2), resulting in constitutive activation of the mammalian target of rapamycin (mTOR) pathway. As a result, the downstream pathways of mTOR become unregulated and ultimately cause uncontrolled growth, enhanced proliferation and migration [1] of smooth-muscle like cells in the lungs [2]. LAM is also associated with increased growth of lymphatic vessels, thought to be partially caused by the increased expression of VEGF receptor-3 (VEGF) on LAM cells, in conjunction with increased serum levels of VEGF-C and -D in LAM patients as a result of the constitutive activation of mTOR. LAM cells located in close proximity to the lymphatic system in the lungs can therefore disseminate and spread via the lymphatic system to other organs such as the kidney, liver and lymph nodes forming extra pulmonary LAM [2]. LAM mainly affects women during their reproductive years [3], with the majority of symptoms being related to breathing difficulties [4], cough and chest pains [5] or in worse conditions, pneumothorax (collapsed lung) [4]. While there is currently no cure for LAM, the disease progression is reduced by rapamycin: an oral macrolide antibiotic drug that acts by inhibiting the mTOR pathway. Since rapamycin's approval by the US FDA in 2014, it has greatly improved the quality of life of LAM sufferers. However, rapamycin is limited by its low oral bioavailability of approximately 15% [6], requiring patients to take large doses of rapamycin to reach a therapeutic effect, which in turn results in unpleasant side effects such as hypertension, respiratory infections and lymphedema and ultimately noncompliance to treatment [7,8].

We have previously shown that delivering nebulized rapamycin encapsulated in solid lipid nanoparticles (Rapa-SLNs) resulted in a more sustained *in vitro* release and transport through the pulmonary epithelium, as well as a more potent inhibition of the enhanced proliferations in LAM cells [9]. Pulmonary delivery thus seems to address the major limitations of oral rapamycin by allowing direct delivery to the site of LAM cell growth and

increasing its *in vivo* half-life [10]. The lymphatic network is present throughout the lungs, running parallel to the major airways down to the alveoli, as well as underneath the surface of lungs [11], thus there is a large surface area available for lymphatic targeting via inhalation of rapamycin to reach extrapulmonary LAM. Previous research have shown that nanoparticles of different compositions (nanocapsules [12], solid lipids [13] and liposomes [14], ranging from 50 to 900 nm [15,16]) can enter the lymphatics via the lungs. Several studies have also demonstrated that nanoparticles with a negative surface charge enhance lymphatic targeting [17–19], while others have reported that a positive surface charge results in increased lymph node retention [20,21]. It is possible that different particle surface charges and size could play different roles in terms of lymphatic targeting, depending on the area of the body through which the nanoparticles are delivered. Surface charge may also be important for improved delivery efficacy. Using positively charged chitosan as a surface decorator for selenium nanoparticles has been shown to improve uptake of selenium by cancer cells and thus amplified anticancer efficacy [22]. Conversely, negatively charged silver nanoparticles showed significantly more antibacterial activity compared with normal silver nanoparticles [23]. The first part of this study showed that Rapa-SLNs of approximately 200 nm in size were able to penetrate through human lymphatic endothelial cells (HLECs) more efficiently compared with larger-sized Rapa-SLNs and free rapamycin [24]. This second part of the study will therefore focus on characterizing the impact of Rapa-SLN charge on their lymphatic entry through the lungs, in comparison to free rapamycin. The effects of surface charge by adding surface modifying agents to the original negative Rapa-SLNs are systematically characterized. Different Rapa-SLNs, produced using two surface charge additives to obtain positive, neutral and negative Rapa-SLNs were evaluated in terms of their physical–chemical characteristics and ability to penetrate through the respiratory epithelium and inhibit the enhanced proliferation of LAM cells. *In vitro* testing on a previously characterized HLECs was also performed, in order to establish the formulations toxicity profiles on HLECs, transport through the monolayer and efficacy on inhibiting lymphangiogenesis.

## Materials & methods

### Materials

Rapamycin (98% w/w purity) was purchased from Hangzhou ICH Biofarm Co. Ltd. (Hangzhou, China), Tween 80 and mannitol from Sigma-Aldrich (Sydney, Australia). Glycerol behenate (Compritol 888) was a gift from Gattefosse (Trapeze Associates Pty Ltd, Sydney, Australia). Chemicals used such as ethanol, methanol and dichloromethane were HPLC grade and purchased from Thermo Fisher Scientific (Australia). Calu-3 cells were bought from American Type Culture Collection (ATCC; VA, USA), while TSC2 mice embryonic fibroblasts (MEF; negative and positive) were a gift from David Kwiatkowski (Brigham and Women's Hospital, MA, USA). Cell culture material including Dulbecco's Modified Eagle's media with phenol red (DMED), high-glucose DMEM, phosphate-buffered saline (PBS) nonessential amino acid solution, CelLytic™ M Cell Lysis solution, Hank's balanced salt solution (HBSS) and trypsin EDTA were all purchase form Sigma-Aldrich. Fetal bovine serum (FBS), L-glutamine solution (200 nM) were bought from Invitrogen (Sydney, Australia), and CellTiter 96R Aqueous One Solution Cell Proliferation Reagent A (MTS) was supplied by Promega (Sydney, Australia). Cell culture plates with transwell insert (0.33 cm<sup>2</sup> polyester, 0.4-um pore size) and 12-well plates (flat-bottom polystyrene) were bought from Corning Costar (MA, USA).

### Rapa-SLNs preparation

Rapa-SLNs with different surface charges were prepared using a hot homogenization method as previously described [9]. In brief, rapamycin and lipid, glyceryl behenate (200 mg, Compritol 888), were dissolved in methanol and dichloromethane, respectively, before the organic solvents were evaporated using the rotary evaporator (RV8, IKA Rotary Evaporator) at 120 rpm, 40°C and a pressure of 600 mbar. A surfactant solution of hot (70°C) aqueous Tween 80 (1.5% w/v) was subsequently added to the lipid–drug film. To obtain Rapa-SLNs with different surface charges, the lipid–drug-surfactant solution was supplemented with different charge-modifying additives, as previously reported in a study by Platel *et al.* [25]. The FDA-approved polyethylene glycol 2000 (PEG2000; 37% w/w) [26], amphiphilic in nature, was used to neutralize the negatively charged Rapa-SLN and produce the same formulation with a neutral surface. Eight percent (w/w) of hexacyltrimethylammonium bromide (CTAB) was used as a cationic additive [25] to produce positively charged Rapa-SLNs, while the negatively charged Rapa-SLN formulation received no additive. All three formulations were subsequently homogenized (ultraturrex, T25) under sheer pressure at 17,000 rpm and 70°C for 15 min. The resulting lipid–drug-surfactant mixture was cooled on ice until reaching room temperature. Finally, 5% (w/v) mannitol was added to all three resulting Rapa-SLNs before

they were snap-frozen in liquid nitrogen and freeze-dried (B. Braun, Melsungen, Germany) overnight (24 h) at  $-50^{\circ}\text{C}$ , as previously reported by Landh *et al.* [9].

### Physicochemical characterization of Rapa-SLNs

#### *Particle size analysis & surface charge*

Dynamic light-scattering analysis (Nano SZ Zetasizer, Malvern Instruments) was used to evaluate the different Rapa-SLNs average particle size, polydispersity index and surface charge. Briefly, freeze-dried Rapa-SLN powder was resuspended in deionized water (25 mg/ml) and PBS, sonicated for 30 min prior to sampling. Each separate formulation was analyzed in triplicates.

#### *Encapsulation efficiency*

The amount of rapamycin encapsulated in the lipids for each formulation (encapsulation efficiency) was determined by measuring the amount of free rapamycin left in aqueous media after centrifuging (4000 rpm) each powder using ultracentrifugal filters (Millipore, USA) for 15 min (tests performed in triplicates). The resulting filtrates were subsequently collected from the supernatant (unfiltered) and precipitate (free drug) of the filtration tubes before being analyzed for rapamycin content using an established HPLC method. The encapsulation efficacy for each formulation was then calculated using the following formula:

$$\text{Encapsulation efficiency (\%)} = \frac{\text{Unfiltered Rapamycin} - \text{Filtered Solution (free drug)}}{\text{Unfiltered Rapamycin}} \times 100$$

#### *Differential scanning calorimetry*

Differential scanning calorimetry (DSC-1; Mettler-Toledo Ltd, Switzerland) was used to assess the thermal properties of the positive and neutral Rapa-SLN formulations compared with the individual charge-inducing additives, CTAB and PEG2000 to confirm the presence of the charge-modifying agents. Briefly, 7 mg samples were weighted and sealed into an aluminum pan that is subsequently pierced with a 1-mm pinhole to ensure pressure equilibrium. The samples were heated at a rate of  $5^{\circ}\text{C}/\text{min}$  from 25 to  $350^{\circ}\text{C}$  under  $\text{N}_2$  atmosphere pressure. STAR V11.0~ software (Mettler-Toledo Ltd) was used to determine the temperatures and onset of each exothermic and endothermic peak. The data were also normalized for initial mass.

#### *Quantitative HPLC*

Rapamycin quantification throughout this study was determined using a validated HPLC (Shimadzu, Sydney, Australia) system equipped with a LC20HT pump, SIL20AHT autosampler and a SPD-20A UV-Vis detector, using a reverse phase C-18 column (Phenomex, ODS hyperclone)  $250 \times 4.6$  mm long and  $5 \mu\text{m}$  particle size. The analysis was performed using a detection wavelength of 278 nm, injection volume of 100  $\mu\text{l}$ , flow rate of 1.2 ml/min and a mobile phase consisting of methanol:water (80:20 v/v). The standard curve for rapamycin was determined for the concentration range of 0.01–50  $\mu\text{g}/\text{ml}$  with a linear regression value of more than 0.999 and a retention time of 9 min. All standard solutions were prepared fresh daily in mobile phase prior to use.

#### *In vitro drug release profile*

The dialysis bag (MW cutoff: 6000–8000, CelluSep, TX, USA) membrane technique was used to evaluate the drug release profiles of rapamycin from the different SLNs with different charge, compared with free rapamycin. The Rapa-SLNs were suspended in PBS (10  $\mu\text{g}/\text{ml}$ ) and made up to 1 ml, while the free rapamycin was first dissolved in DMSO before diluted in PBS to make up 1 ml, with DMSO being less than 0.1% (w/v) of the total volume. Subsequently, 1-ml samples of each formulation/drug solution, prepared in triplicate, were placed in separate dialysis bags and immersed into 60 ml of PBS to ensure sink conditions. The dialysis bag system was kept under constant stirring at  $37^{\circ}\text{C}$ , with samples withdrawn from the basal media every hour for up to 4 h and replaced with equal amount of PBS at each time point. The collected samples were quantified for rapamycin content using HPLC. Each formulation/drug condition was performed in triplicate.

### Transepithelial drug transport studies across respiratory epithelium

To investigate the transport of different charged Rapa-SLNs compared with free rapamycin through the respiratory epithelium, an established air interface model of the bronchial epithelial cells was used. Briefly, bronchial epithelial

Calu-3 cells were purchased from ATCC (MD, USA), and were cultured in DMEM containing 10% (v/v) FBS, 1% (v/v) L-glutamine and 1% (v/v) nonessential amino acids. The cells were maintained in humidified incubators (95% air and 5% CO<sub>2</sub>) at 37°C with the media changed every 2–3 days and passaged when reaching 95% confluence, according to the manufacturer's guidelines. Subsequently, Calu-3 cells were cultured at a density of  $5 \times 10^5$  cells/cm<sup>2</sup> on polystyrene transwell inserts (pore size = 0.4 μm). To establish an air–liquid interface cell model, cells were cultured between 11 and 14 days before with the apical media removed after 24 and 48 h post-seeding to expose the cells to air [27].

For the transport study, free rapamycin and the different Rapa-SLNs (13.1 μg/ml) were resuspended in HBSS and nebulized via a Pari jet nebulizer, onto the cells using a modified twin-stage liquid impinger (British Pharmacopeia Apparatus A, Copley Scientific) [28] at a flow rate of 15 l/min for 15 s, as previously described [9]. Subsequently, the transwells were placed into a clean 24-well plate with 500 μl of HBSS at the basolateral chamber and incubated in a humidified (37°C, 5% CO<sub>2</sub>) chamber for 4 h. Samples were withdrawn from the basolateral chamber after 30, 60, 120, 180 and 340 min postdeposition and replaced with equal amounts of HBSS each time. The amount of drug remaining on the surface of the cells after 4 h was determined by washing the apical surface of the transwells with HBSS multiple times and collecting the samples for quantification. The amount of drug remaining inside the cell at the end of the experiment was determined by first adding HBSS to the apical chamber, before scratching the membrane using a pipette tip to detach the epithelial cells from the transwells. Collected samples were then centrifuged at 13,000×g for 5 min, before the supernatant was discarded and cell lysis buffer added. An insulin syringe was then used to rupture the cell membrane to release the intracellular drugs. Samples were centrifuged again to ensure the removal of cell debris and the supernatant analyzed for rapamycin content using the HPLC.

Transepithelial electrical resistance (TEER) across the epithelium was also measured before and after treatments to ensure the treatment has no effect to the integrity of the epithelium. Briefly, TEER measurements were performed using an EVOM voltohmmeter (World Precision Instrument, FL, USA) connected to STX-2 chopstick electrodes and measurements taken by inserting the longer chopstick end into the basolateral chamber and the shorter chopstick end into the apical chamber, hence measuring the potential resistance differences between the two chambers. TEER values were calculated by subtracting the resistance readings of blank inserts from the test readings and multiplying it by the transwell insert area (0.33 μm). TEER experiment was performed in triplicates for each treatment.

### Proliferation assay on MEF cells

A proliferation assay was performed using TSC2 positive and negative MEF cells to evaluate the ability of the charged Rapa-SLNs to inhibit the proliferation of LAM-like cells. Both TSC2 negative and positive MEFs were cultured in high-glucose DMEM media containing 10% (v/v) FBS and 1% (v/v) penicillin–streptomycin and maintained in humidified incubator (95% air and 5% CO<sub>2</sub>) at 37°C with the media changed every 2–3 days and passaged when reaching 95% confluence, according to the respective manufacturer's guidelines.

The TSC2 positive and negative MEF cells seeded at a density of  $1 \times 10^4$  cells/cm<sup>2</sup> in serum-reduced media (0.5% v/v FBS). Cells were incubated in a humidified atmosphere (5% CO<sub>2</sub>) for 24 h before proliferation was induced by treating cells with different concentrations (0.2–200 nM) of free rapamycin and different-sized Rapa-SLNs (200, 500 and 1000 nm) in the presence of 10% (v/v) FBS media. After 24 hrs of incubation following treatment, cells were trypsinized and counted using a Scepter cell counter (Merck Millipore, Darmstadt, Germany) to establish the number of viable cells.

### Effect of Rapa-SLN surface charge on HLEC

HLECs were cultured in endothelial cell media containing 5% (v/v) FBS and 1% (v/v) EC growth supplements and 1% (v/v) penicillin–streptomycin and maintained in a humidified incubator (95% air and 5% CO<sub>2</sub>) at 37°C. The cells were subcultured in fibronectin (2 μg/cm<sup>2</sup>) coated 75 cm<sup>2</sup> flasks with the media changed every 2–3 days and passaged when reaching 95% confluence, according to the respective manufacturer's guidelines.

### Cell toxicity assay

To evaluate the toxicity of the different Rapa-SLNs on HLECs, a range of concentrations (0.001–100 μM) of each nanoparticle formulation and free rapamycin were prepared separately in culture medium, and tested on the HLECs. Each freeze-dried Rapa-SLN formulation was initially suspended in PBS, while the free rapamycin was first dissolved in DMSO before further dilution in culture media to a stock solution containing less than 1% v/v DMSO. HLECs were seeded at a density of  $1.2 \times 10^4$  cells/cm<sup>2</sup> in fibronectin-coated 96-well polystyrene

flat-bottom plates and incubated at 5% CO<sub>2</sub> and 37°C overnight before the addition of drug treatments. Treated cells were further incubated in a humidified chamber and assessed for viability after 72 h. Viability was assessed by adding 20 µl of Aqueous One Solution Proliferation Agent (Promega) to each well prior to incubation for a further 4 h. The fluorescence of each well was then measured at 490 nm using a fluorescence microplate reader (Spectromax M2; Molecular Devices, USA). Cell viability was calculated as a percentage of viable cells compared with untreated controls and the IC<sub>50</sub> values were calculated by applying the inhibitory dose-response curve to the plotted data using the GraphPad Prism 7.0.

#### *Tube formation assay*

To evaluate the effects of Rapa-SLNs surface charge on the formation of new lymphatic vessels, a tube formation assay was performed as described previously [29,30]. Briefly, HLECs were seeded at a density of  $1.2 \times 10^4$  cells/cm<sup>2</sup> on fibronectin-coated (2 µg/ml) 12-well plates. Cells were then pretreated with either 200 nM of free rapamycin, negative Rapa-SLNs, neutral Rapa-SLNs or positive Rapa-SLNs, and incubated for 24 h. Subsequently, a 96-well plate was precoated with 40 µl of matrigel (10 µg/ml) per well and incubated at 37°C for 40 min to ensure complete solidification of the matrigel. Next, the pretreated cells were trypsinized and seeded onto the matrigel plates at a density  $2 \times 10^4$  cells/well in presence of the different drug treatments before being incubated for a further 6 h at 37°C. Cells were then imaged using Nikon time Eclipse Ti-microscope (Nikon, Eclipse Ti, Tokyo, Japan) and ImageJ software was used to quantify tube length, measuring its length in pixels. The average of three randomly selected fields of views within each treatment was used to calculate the average length within each different treatment condition.

#### *Drug transport assay on HLEC*

Transport of the different Rapa-SLNs compared with free rapamycin across the lymphatic vessels was investigated via a transport assay study using confluent HLEC layer that was established in Part 1 of the study. Briefly, HLECs were seeded at a density of  $5.3 \times 10^4$  cells/cm<sup>2</sup> onto fibronectin (2 µg/ml) coated 96-well polycarbon transwells (pore size = 0.4 µm). Cells were incubated in a humidified chamber (5% CO<sub>2</sub>) at 37°C for 72 h to ensure the formation of a confluent monolayer. After incubation, cell inserts were placed in a new clean 96-well plate with 240 µl of HBSS in each basolateral compartment. Subsequently, free rapamycin and Rapa-SLNs (13 µg/ml) were resuspended in HBSS and 80 µl added to the apical compartment of the transwells, for each treatment condition. Cells were incubated further at 37°C for 4 h with samples removed from the basolateral chamber every hour and replaced with equal amounts of HBSS each time. Samples were quantified for rapamycin content using HPLC. The apparent permeability (Papp) of the different formulations through the endothelial layer was calculated to establish the amount transported through using the formula for Papp coefficient  $Papp = (dQ/dt) \times (1/AC)$ , which stands for:  $Papp = (\text{change in concentration}/\text{change in time at steady state}) \times (\text{the growth area plate chamber}/\text{initial concentration in the apical chamber})$ .

Transport of sodium fluorescein (Na-Flu) across the endothelium was performed following each treatment to assess the integrity of the HLEC monolayer. Transwells were placed into a clean 96-well plate with 240 µl of fresh HBSS in the basolateral compartment. Eighty microliter Na-Flu (2.5 mg/ml) was then added to the apical compartment of each transwell before being incubated at 37°C and 5% CO<sub>2</sub>. Samples were removed from the basolateral chamber every 20 min for 1 h and replaced with equal amount of HBSS each time. A fluorescence plate reader (Spectramax M2; Molecular Devices) was used to measure the fluorescence of the collected samples at excitation and emission wavelengths of 485 and 520 nm, respectively. The apparent permeability (Papp) of Na-Flu through the HLECs was then calculated for each different treatment as outlined by the formula above and compared with untreated control cells.

#### **Statistical analysis**

All experimental data are expressed as mean ± SD and/or mean ± SEM, as indicated, of a minimum of three independent replicates. To establish statistical significance, data were analyzed using two-tailed unpaired t-test or one-way ANOVA, with significant level determined at  $p < 0.05$  and compared with control groups or vehicle controls, as indicated.

**Table 1. Summarized particle characterizations of the differently charged rapamycin solid lipid nanoparticles.**

Rapa-SLNs	Particle size (nm)	Polydispersity index	Surface charge (potential)	Encapsulation efficacy (%)
A: Negative	237.5 ± 1.8	0.4 ± 0.1	-18.1 ± 0.03	97.3 ± 1.3
B: Neutral	201.3 ± 1.2	0.3 ± 0.2	-1.2 ± 0.04	95.1 ± 2.4
C: Positive	220.5 ± 0.7	0.4 ± 0.4	+ 46 ± 0.2	96.2 ± 2.1

Rapa-SLN: Rapamycin solid lipid nanoparticle.

## Results & discussion

The present study aimed to systematically investigate the effect of Rapa-SLNs' surface charge on its ability to enter the lymphatic system via the lungs. Therefore, three Rapa-SLNs with different surface charge were first characterized for their *in vitro* release profiles and ability to permeate the respiratory epithelium and lymphatic endothelium. Second, the formulations were also compared for their efficacy against LAM by evaluating their ability to inhibit the enhanced proliferative properties of LAM-like cells and tube formation of HLECs.

### Manufacture & characterization of Rapa-SLNs with different surface charges

#### *Physical characterization of Rapa-SLNs*

Particle characterization (Table 1) showed that using a hot evaporation technique and different surface modifying additives resulted in three Rapa-SLNs with different surface charge. The presence of the charge-modifying agent CTAB, resulted in Rapa-SLNs with a positive surface charge (Formulation C) of  $46 \pm 0.2$ ; while the addition of PEG2000 resulted in Rapa-SLNs with a neutral surface charge (Formulation B) of  $-1.2 \pm 0.4$ . The original Rapa-SLN formulation produced with the presence of no extra additive resulted in Rapa-SLNs with a negative surface charge (Formulation A) of  $-18.1 \pm 0.03$  (Table 1). The negative charge on the original formulation can mainly be attributed to the presence of the lipid carrier Compritol 888. The hydrophobic lipid carrier is based on behenic acid, and consists of mono-, di- and triglycerol esters [31,32]. The negative surface charge is most likely due to the ionization of the carboxyl group on the glyceryl behenate, as it has been shown that increasing the concentration of glyceryl behenate results in decreased surface charge [33]. In contrast, the presence of the nonionic surfactant Tween 80 (polysorbate 80, polyoxyethylene sorbitan monooleate) is unlikely to have impacted significantly on the surface charge of the original formulation, due to its low percentage (1.5% w/v) within the total lipid–drug matrix. While previous studies have shown that increasing the concentration of Tween 80 in the presence of glyceryl behenate can increase the  $\zeta$  potential of the overall SLNs by ionizing the solid lipid functional groups [33]. It has also been shown that increase in chain lengths of surfactant (Tween 80) increases hydrophobicity and thereby results in a more dense firmer solid lipid, as the hydrophobic chains are arranged more closely, thereby increasing the stability of the SLNs as well as the surface charge [34]. However, increasing the concentration of glyceryl behenate while decreasing the concentration of Tween 80 has also been shown to result in a more negative  $\zeta$  potential and surface charge, as not enough surfactant was present to ionize the complete solid lipid [33], which seems to be the case in the present study where Tween 80 was used at a ratio of 1.5% (v/v) and the final  $\zeta$  potential was negative. Additionally, the active drug rapamycin encapsulated in the solid lipids may have contributed to the overall surface charge as it is very hydrophobic, and has electronegative nitrogen functional groups in its ring structures [35]. Moreover, the addition of CTAB resulted in a positive surface charge confirming its nature of a cationic-reducing agent [25]. Hence, it most likely acted as a reducing agent to the carboxyl groups of glycerol behenate, and thereby increased the surface charge of the Rapa-SLN formulation. Similarly, the presence of the surface-modifying agent PEG2000, amphiphilic, nonionic in nature, was able to neutralize the negative surface charge of the original formulation to result in a  $\zeta$  potential close to 0 [26].

There were no significant differences in encapsulation efficacy of all three Rapa-SLNs, with more than 95% of the rapamycin being encapsulated within the lipid carrier, and no significant difference in the loading efficiency between the different formulations with each formulation containing an average of 1.31  $\mu\text{g}$  of rapamycin/mg freeze-dried powder. In addition, all three formulations had an average particles size of approximately 200 nm, with polydispersity indexes  $<0.4$ , indicating monodisperse particle distributions as previously shown [13,36].

#### *Thermal properties of the Rapa-SLNs*

Thermal behavior of the positive and neutral Rapa-SLNs and the individual charge-inducing additives, CTAB and PEG2000 were measured using a DCS and displayed in Figure 1. Two endothermic peaks are displayed by raw

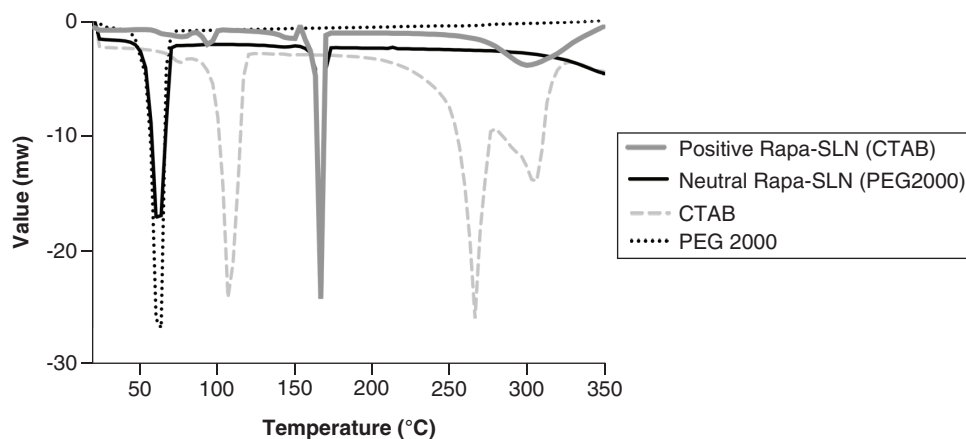


**Figure 1.** Differential scanning calorimetry thermographs of positive and neutral rapamycin solid lipid nanoparticle and their respective unprocessed charge inducing additives, hexacyltrimethylammonium bromide and polyethylene glycol 2000.

CTAB: Hexacyltrimethylammonium bromide; PEG: Polyethylene glycol; Rapa-SLN: Rapamycin solid lipid nanoparticle.

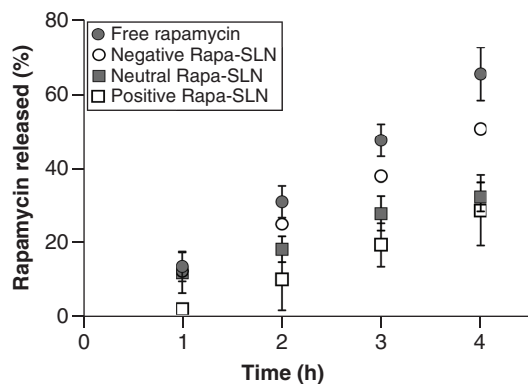


**Figure 2.** *In vitro* drug release profiles of free unencapsulated rapamycin, negative rapamycin solid lipid nanoparticles, neutral rapamycin solid lipid nanoparticles and positive rapamycin solid lipid nanoparticles across a dialysis membrane.  $n = 3 \pm SD$ . Rapa-SLN: Rapamycin solid lipid nanoparticle.

CTAB at 106.6 and 266.6°C, with the first peak most likely arising from the dehydration reaction of CTAB and second peak from the liberation of the organic cations in the sample [37]. The thermal graph of positive Rapa-SLN, which contains the surface additive CTAB, showed two smaller endothermic peaks at similar temperatures, indicating that the CTAB is present within the formulation but interactions are most likely present between the additive and lipid polymer. Two more endothermic peaks are present within the positive Rapa-SLN, a minor one at 150°C and a major one at 160.6°C, which could be attributed to the melting points of the lipid polymer glycerol debehenate and the mannitol, which has been shown by previous research for the Rapa-SLN formulation without the additive present [9].

On the other hand, the thermograph of raw PEG2000 displays a sharp endothermic peak at 63.3°C, which correlates to the melting point of PEG2000 as reported by previous research [38]. The thermal graph of neutral Rapa-SLN, which contains the surface additive PEG2000, displays a similar graph to positive Rapa-SLN but with an extra endothermic peak at 63.3°C corresponding to that of raw PEG2000, thereby showing the presence of the additive within the formulation. Notably, the absence of the endothermic peaks of rapamycin's melting point around 185°C [39,40] within the neutral and positive Rapa-SLN thermographs suggests that the drug has become fully miscible within the formulations.

#### *In vitro drug release profiles of Rapa-SLNs*

Figure 2 shows the release profiles of free rapamycin and the different charged Rapa-SLNs across the dialysis bag. Free rapamycin demonstrated the most rapid drug release, with  $65.3 \pm 7.0\%$  released from the dialysis bag after 4 h, compared with the sustained release displayed by the charged Rapa-SLNs with negative, neutral and positive Rapa-SLNs releasing approximately  $50 \pm 1.9\%$ ,  $32.4 \pm 3.9\%$  and  $28.7 \pm 9.6\%$ , of rapamycin, respectively. The

**Table 2. Similarity ( $f_2$ ) and difference factors ( $f_{1[1/toxarisitalic]}$ ) for rapamycin solid lipid nanoparticles with different charge compared with free rapamycin.**

Rapa-SLNs	$f_1$	$f_2$
Positive	61.6	29.2
Neutral	42.6	34.6
Negative	20.0	51.5

The profiles are deemed different if  $f_1 \geq 10$  and  $f_2 \leq 50$ .  
Rapa-SLN: Rapamycin solid lipid nanoparticle.

Rapa-SLNs and the reference-free rapamycin were analyzed and compared using similarity and difference factors from the fit factor analysis model (Table 2). The fit factor analysis is based on a mathematical model by Moore and Flanner, which assigns the release profiles a difference factor ( $f_1$ ) and similarity factor ( $f_2$ ) where two profiles are deemed different when  $f_1 \geq 10$  and  $f_2 \leq 50$  [41]. Results show that the release profiles of rapamycin from the neutral and positively charged Rapa-SLNs are significantly different to the free rapamycin, while the negatively charged Rapa-SLNs had a difference ( $f_1$ ) factor  $>10$  but a borderline similarity ( $f_2$ ) factor of 51.5 compared with the free unencapsulated rapamycin.

Overall, the positive surface charge of the Rapa-SLNs resulted in the slowest drug release compared with the other formulations. Regardless of charge, all three Rapa-SLN formulations resulted in a more sustained release of rapamycin compared with the free unencapsulated drug. Drugs can generally be released from polymer nanoparticle matrix via diffusion or polymer erosion. In this instance, the mechanism is likely to occur via diffusion with the presence of surface-modifying agents in the neutral and positive SLNs acting to slow down the release of rapamycin [42]. In the case of CTAB, which consist of an alkyl chain and an ionic polar head group [42], which acts to add charge to the lipid–drug matrix, compared with the original formulation. Thereby, the electronegative drug is held tighter to the lipid matrix making it less susceptible to hydration in an aqueous environment, resulting in slower release of the drug particles [43]. Similarly, the surface-modifying agent PEG2000, nonionic in nature, masks the carboxyl end groups of the original formulation [44], holding the drug tighter to the matrix and reducing its susceptibility to hydration. While the original negative Rapa-SLNs would be more susceptible to hydration, leaving open the surface hydrophilic framework of the SLNs, increasing the penetration of the aqueous media and dissolution of the hydrophilic end groups of the lipid, ultimately resulting in faster release of the drug from the SLNs matrix [45].

### Surface charge investigation of Rapa-SLNs on transport across the respiratory epithelium

To investigate the ability of the different charged Rapa-SLNs to access the lymphatic system via inhalation, their ability to transport through the airway epithelium prior to reaching the neighboring lymphatic system was investigated. In the pulmonary lymphatic system, lymphatic vessels run in parallel to the major airways and conducting bronchioles all the way to the interalveolar walls [11]. Additionally, pleura covering the lungs consist of a subpleural lymphatic network [11]. We have previously shown that *in vitro* aerosol performance studies of Rapa-SLNs delivered via nebulization had a mass median aerodynamic diameter of  $5.4 \pm 0.4 \mu\text{m}$  and fine particle fraction of  $44.1 \pm 5.1\%$ , making the formulation highly likely to be deposited in the bronchial region of the airways [9]. Therefore, the differently charged formulations ability to cross the mucous lined respiratory epithelium was assessed through an established air–liquid interface model of Calu-3 cells [46,47] using nebulization.

Results showed that the charged Rapa-SLNs were transported across the epithelium at a faster rate, where the positive and negative Rapa-SLNs transporting  $65.7 \pm 5.7$  and  $59.1 \pm 2.1\%$  rapamycin across the epithelium, respectively. In contrast, the neutral Rapa-SLNs and free rapamycin transported  $44.6 \pm 3.8$  and  $49.8 \pm 2.4\%$  rapamycin over 4 h, respectively. Additionally, the fit factor analysis revealed that there was a statistical difference between the positive Rapa-SLN formulation and the free rapamycin (Figure 3A & B). Furthermore, it was found that negative Rapa-SLNs had the lowest amount of drug inside the cells, with  $11.4 \pm 1.5\%$  rapamycin recovered at the end of the 4 h experiment, while the free rapamycin had the highest amount with  $32.6 \pm 0.6\%$  recovered. While the positive and neutral Rapa-SLNs had  $25.4 \pm 5.7\%$  and  $28.6 \pm 4.8\%$  rapamycin recovered, respectively. On the other hand, the neutral and positively charged Rapa-SLNs instead had the highest amount of rapamycin remaining on surface of the epithelium after 4 h with  $50.3 \pm 11.1\%$  and  $37.4 \pm 9.6\%$  recovered, respectively;

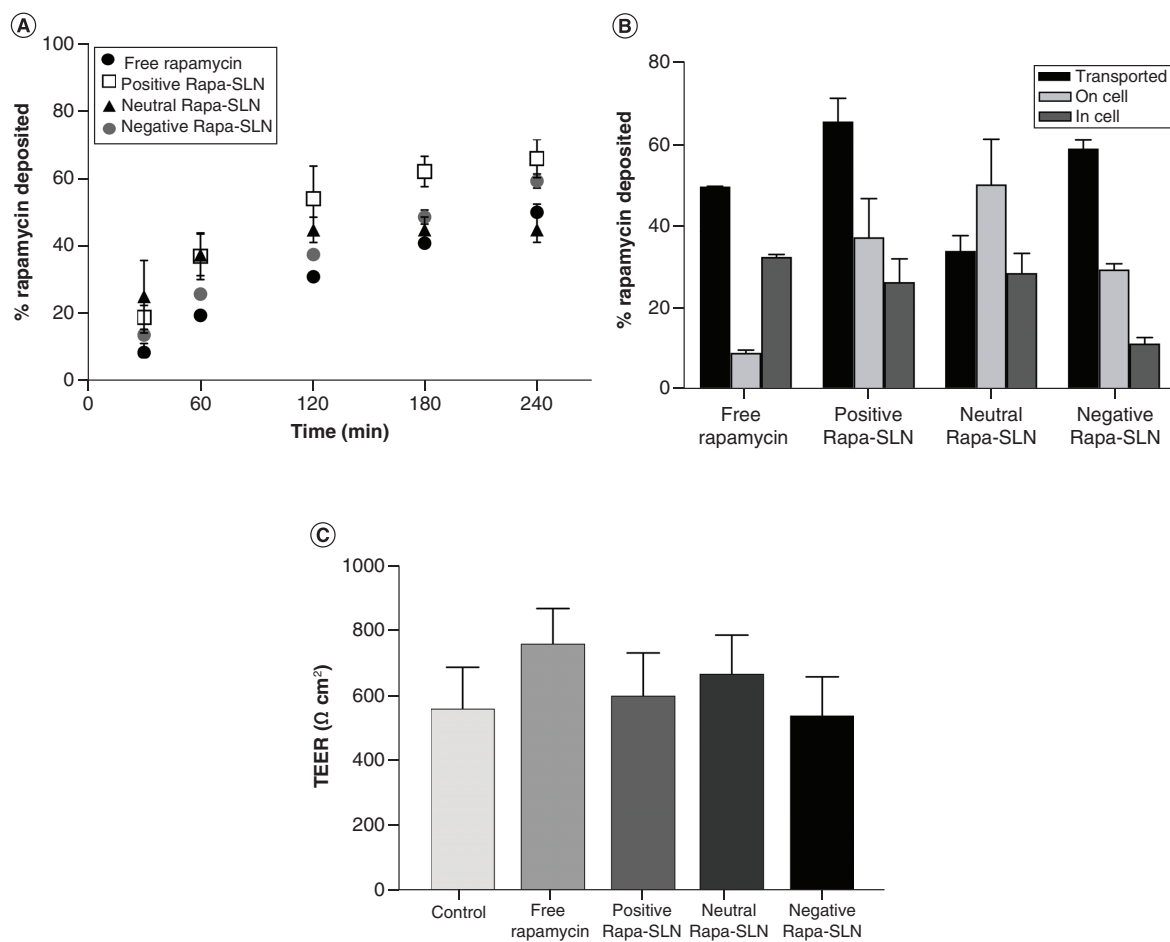


**Figure 3. Transport across the respiratory epithelium. (A)** Transport of free rapamycin, positive Rapa-SLNs, neutral Rapa-SLNs and negative Rapa-SLNs across Calu-3 epithelial cell layer as a function of time. **(B)** Percentage of rapamycin from different Rapa-SLNs recovered ON the cells, IN the cells and transported across the epithelial cell layer, 4 h after deposition. **(C)** Transepithelial electrical resistance of the epithelial barrier of untreated control cells compared with cells treated with the different Rapa-SLNs. Data expressed as the mean of three independent measurements  $\pm$  SD. Rapa-SLN: Rapamycin solid lipid nanoparticle; TEER: Transepithelial electrical resistance.

while the negative Rapa-SLNs and free rapamycin having  $29.5 \pm 1.4\%$  and  $9.1 \pm 0.7\%$  remaining on the surface, respectively.

These differing transport rates and intracellular accumulation of free drug, charged and noncharged SLNs is likely due to the transport pathway of the nanoparticles across the epithelium. The mucous layer covering the epithelium is made up of charged glycoproteins and water, which overall makes it hydrophilic in nature [48]. It is therefore easier for the charged hydrophilic Rapa-SLNs (positive and negative) to move through the mucous layer, as they encounter electrostatic attraction with the charged mucous, compared with the neutral Rapa-SLNs. The same applies to the free rapamycin, which is a hydrophobic uncharged drug that would find it difficult to get transported through the charged mucous layer. Furthermore, it has been well documented that hydrophilic drugs with a net charge are primarily transported across the epithelium via the paracellular route through tight junctions, compared with the hydrophobic uncharged drugs, which tend to pass through via the transcellular route [49]. This also supports the finding of higher accumulation of free rapamycin and neutral Rapa-SLNs within the cells compared with the negative Rapa-SLNs in the transport experiment.

While it is likely that the majority of the Rapa-SLNs crossed the epithelium via the paracellular route, the accumulation of a small portion of the negative Rapa-SLN and larger portion of the positively charged formulation, inside the epithelium after 4 h indicate that a percentage of these formulation also crossed the cell via the transcellular route. Bannunah *et al.* showed that negatively charged nanoparticles had a higher transport efficiency

across intestinal Caco-2 cell epithelium layer compared with similar sized positively charged particles, even though the positively charged particles had a higher level of internalization [50]. These findings have been explained by positively charged particles exhibiting higher cell internalization rate compared with the negative SLNs due to their different interactions with the membrane. The epithelial membrane displays a net negative surface charge due to the presence of negative-charged extracellular plasma proteins [51], which may promote positively charged particles to interact electrostatically with the membrane to a greater extent than the negatively charged particles [50]. This, in turn, would induce endocytosis more rapidly for the positive SLNs compared with the negative SLNs, as well as the neutral one [52]. Different translocation pathways taken by the differently charged SLN formulation could also explain the different levels of accumulation within the cell layer. Previous research has also shown that transport of positively charged nanoparticles across the epithelium is mainly governed by the clathrin-mediated pathways [53], while negatively charged particles are mainly transcytosed via the caveolae-mediated pathway [53,54]. In our study, charged Rapa-SLNs with positive or negative surface charges resulted in efficient transport across the bronchial epithelium compared with free rapamycin and neutral Rapa-SLNs. In addition, it was found that there was no significant difference in the TEER measurements (Figure 3C) between the treated cells and control cells, which showed that neither the Rapa-SLNs or the free rapamycin had an effect on the integrity of the epithelium and the tight junctions that could have impacted on the transport of the rapamycin across the epithelium.

### Rapa-SLNs inhibit induced proliferation in TSC2-negative MEFs

A major therapeutic benefit of rapamycin is its ability to reduce the enhanced proliferation of LAM cells in the lungs and other parts of the body. Previous research have studied the effect of rapamycin in TSC2-negative MEF cells, which are p52 knockouts and dysfunctional for the *TSC2* gene that mimics the disease state of LAM cells. These studies have shown that free rapamycin at a concentration of 20–200 nM can significantly inhibit the increased proliferation of TSC2-negative MEF cells, while having no effect on the normal wild-type TSC2-positive MEF cells [55,56].

In the present study, the TSC2-positive and -negative MEF cells were therefore treated with increasing doses of 0.2–200 nM of rapamycin from the different Rapa-SLNs. The results (Figure 4B) showed that the complete dose range of both the positively and negatively charged Rapa-SLNs significantly ( $p < 0.05$ ) inhibited the increased proliferation in the TSC2-negative MEFs, compared with the vehicle control. The neutral Rapa-SLNs, however, did not result in a significant reduction in proliferation compared with the vehicle control. Similar results over the same concentration rate of Rapa-SLNs have been demonstrated in our previous study [9]. Thus, these findings further support that charge has an effect on the ability of the nanoparticles to enter into the MEF cells, where the anionic and cationic surface charges appear to have an equal effect at inhibiting proliferation compared with the neutral. As previously demonstrated that rate of uptake of different charged SLNs is influenced by cell membrane's properties that have an overall slight negatively charge [57,58]. This property has shown to promote positively charged nanoparticles to electrostatically adhere to the cell membrane, resulting in more readily internalization compared with negative and uncharged nanoparticles [59–61]. While both neutral and negatively charged nanoparticles are internalized via endocytic mechanisms to a lower extent to positively charged particles [58], positively charged nanoparticles have also been shown to be internalized through an additional pathway via disrupting the lipid bilayer to create pores [62]. This mechanism of entry by positively charged nanoparticles can at times results in toxic effects and cellular abruptions [62,63], as shown for the higher doses of the positive Rapa-SLNs that resulted in a significant reduction in proliferation of the wild-type TSC2-positive MEF cells (Figure 4A). These effects were not apparent for the negative and neutral Rapa-SLNs, implying that the positive Rapa-SLNs may result in a toxic effect on the cells, rather than a decrease in proliferation, as these cells do not exhibit the dysfunctional gene for enhanced proliferation. Regardless, the charged Rapa-SLNs resulted in a significant decrease in proliferation compared with neutral Rapa-SLN and a more potent decrease in proliferation at lower doses compared with previous results using free rapamycin [55,56].

### The impact of Rapa-SLN surface charge on HLECs

#### *Rapa-SLN is nontoxic against HLECs*

Cytotoxicity of increasing doses (0.001–100  $\mu\text{M}$ ) of the differently charged Rapa-SLNs compared with free rapamycin on HLECs were assessed via metabolic activity assay (MTT assay). Results (Figure 5) showed that the positive- and negative-charged Rapa-SLNs were the most toxic, with  $\text{IC}_{50}$  values of  $0.2 \pm 0.7$  and  $4.9 \pm 0.9$   $\mu\text{M}$ , respectively; while the free rapamycin had an  $\text{IC}_{50}$  value of  $13.2 \pm 0.8$   $\mu\text{M}$ . The neutral Rapa-SLNs was the least

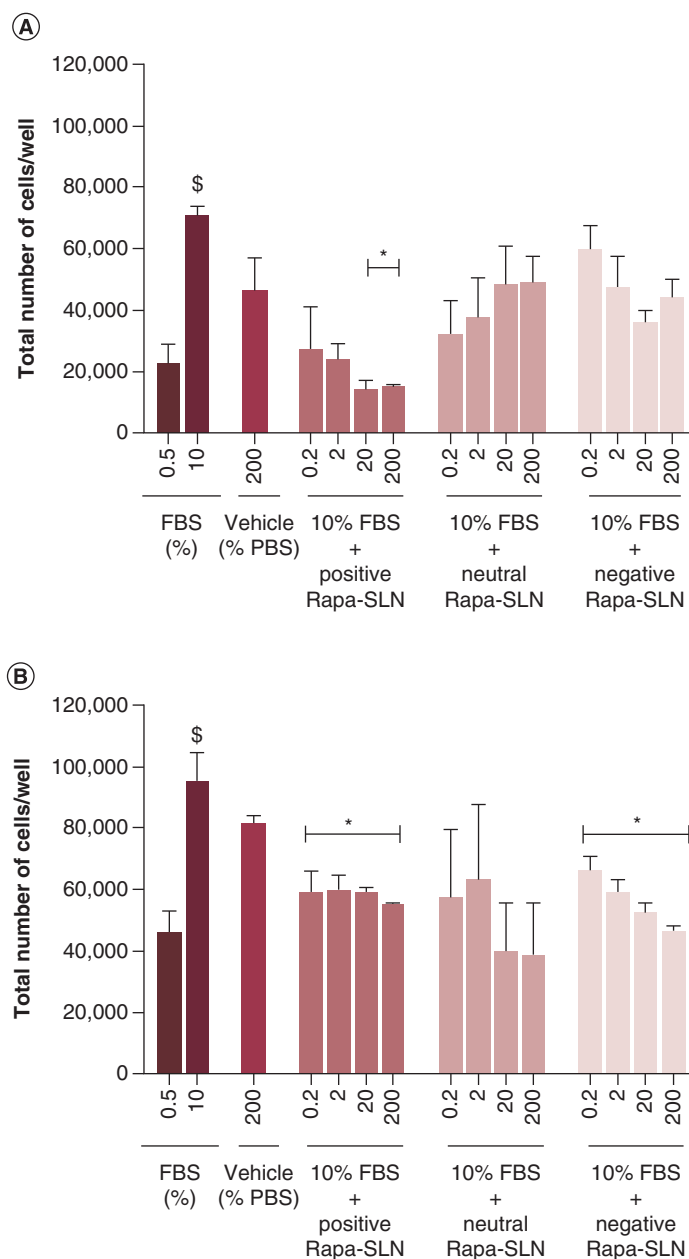


**Figure 4. Proliferation in TSC2 mice embryonic fibroblast cells. (A) TSC2-positive MEFs and (B) TSC2-negative MEFs treated with different concentrations of positive Rapa-SLNs, neutral Rapa-SLNs or negative Rapa-SLNs compared with vehicle controls where appropriate ( $n > 3$ ). Data expressed as means  $\pm$  SD.**

$^{\$}$   $p < 0.05$  compared with 0.5% FBS control;  
 $^*$   $p < 0.05$  compared with PBS vehicle control.

FBS: Fetal bovine serum; PBS: Phosphate-buffered saline; Rapa-SLN: Rapamycin solid lipid nanoparticle.

toxic with an  $IC_{50}$  of  $39.5 \pm 0.9 \mu\text{M}$ . These results also indicate that the positively charged Rapa-SLNs are more toxic than the negative and neutral Rapa-SLNs, as well as the free rapamycin. Based on these results, treatments in subsequent experiments on the HLECs were kept under a dose of  $2.5 \mu\text{M}$  and/or lower exposure time to the drug.

#### *Negatively charged Rapa-SLNs are transported across the HLEC*

The confluent monolayer of HLECs was used as an *in vitro* model to study the transport of the differently charged Rapa-SLNs compared with free rapamycin, into the lymphatic vessels over a 4-h time period. It was found that the negatively charged Rapa-SLNs had the highest permeability through the HLEC compared with free rapamycin ( $p < 0.05$ ), the neutral and positively charged ( $p < 0.0005$ ) Rapa-SLNs (Figure 6). Previous studies demonstrated that negatively charged lipid-based nanoparticles increase uptake into the lymphatics, compared with positive and neutral ones [17,18]. One study injected rats with differently charged liposomes labeled with a  $^{99\text{m}}\text{Tc}$ , a membrane marker, and found a higher retention of negatively charged liposomes, followed in decreasing order by positively and neutral charged liposomes, in the primary and secondary regional lymph nodes 4 h

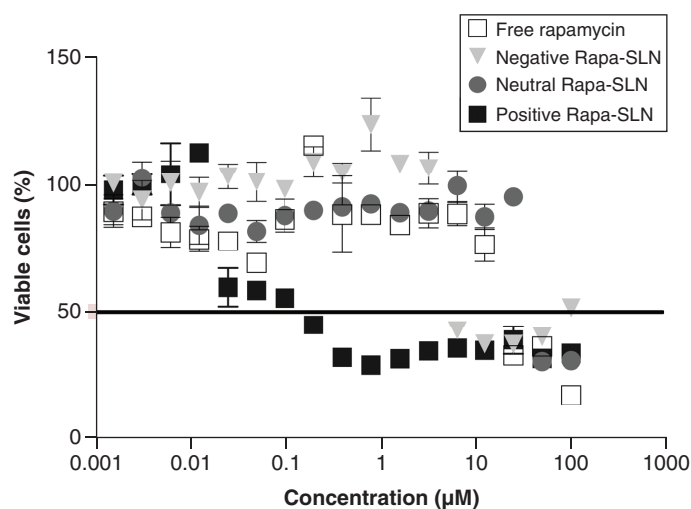


**Figure 5.** Cytotoxicity of increasing doses of free rapamycin, negative rapamycin solid lipid nanoparticles, neutral rapamycin solid lipid nanoparticles and positive rapamycin solid lipid nanoparticles on human lymphatic endothelial cells. Data expressed as percent viable cells versus Log concentration.  $n = 3 \pm SD$ . Rapa-SLN: Rapamycin solid lipid nanoparticle.

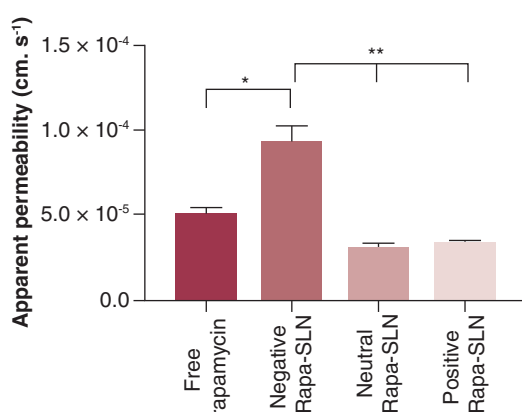


**Figure 6.** Apparent permeability of free rapamycin, negative rapamycin solid lipid nanoparticles, neutral rapamycin solid lipid nanoparticles and positive rapamycin solid lipid nanoparticles, across human lymphatic endothelial cell layer over a 4-h period. Data expressed as the mean of three independent measurements  $\pm SD$ . \* $p < 0.001$ ; \*\* $p < 0.0002$ . Rapa-SLN: Rapamycin solid lipid nanoparticle.

after administration [18]. Similarly, Kauer *et al.* subcutaneously injected rats with Zidovudine-loaded liposomes with different surface charge. Organ distribution analysis showed a higher lymph node concentration of negatively charged liposomes compared with positive ones after 1–4 h [17]. Furthermore, another study by Rao *et al.* investigated the lymph uptake of poly(D,L-lactic-co-glycolic) acid (PLGA-COOH) and poly(ethylene glycol-*b*-D,L-lactic acid) PLGA-PMA conjugated to a fluorescent marker molecule (PMA), allowing tracking of the particles *in vivo* [19]. PLGA-COOH were conjugated to PLGA-PEM in different ratios to create particle systems with different surface charge, while keeping them of similar size ( $\sim 200$  nm). Results showed that there was a direct increase in lymph node uptake with increasing anionic charge over a 24-h period [19]. However, they attributed these findings to the anionic charge resulting in increased macrophage uptake and drainage of the nanoparticles into regional lymph nodes [19]. The enhanced uptake of negatively charged lipid-based nanoparticles has also been attributed to the anionic particles moving faster through the negatively charged interstitium, as they encounter electrostatic repulsion compared with positively charged ones [17–19,64].

The general described route on *trans*-endothelial transport of solutes and fluid through the endothelial layer has been via the paracellular route via cell-to-cell junctions [65]. These cell-to-cell junctions have been shown via electron microscopy studies to be specialized fenestrated overlapping junctions [66–68], which allow fluid and solutes to enter while also preventing backflow [69]. Additionally, recent studies suggested that transcellular vesicular transport via endocytic pathways, by which the particles enter the HLECs, may account for these differences [65]. It has been shown that caveolae-mediated endocytosis is generally favored by negatively charged nanoparticles [70,71], while positively charged particles mainly utilize the clathrin-mediated pathway [72], which may account for the difference in transport rate in the current study. Nevertheless, the present results clearly suggest that a negative surface charge is highly favorable for the transport of Rapa-SLNs through the lymphatic endothelial cells.

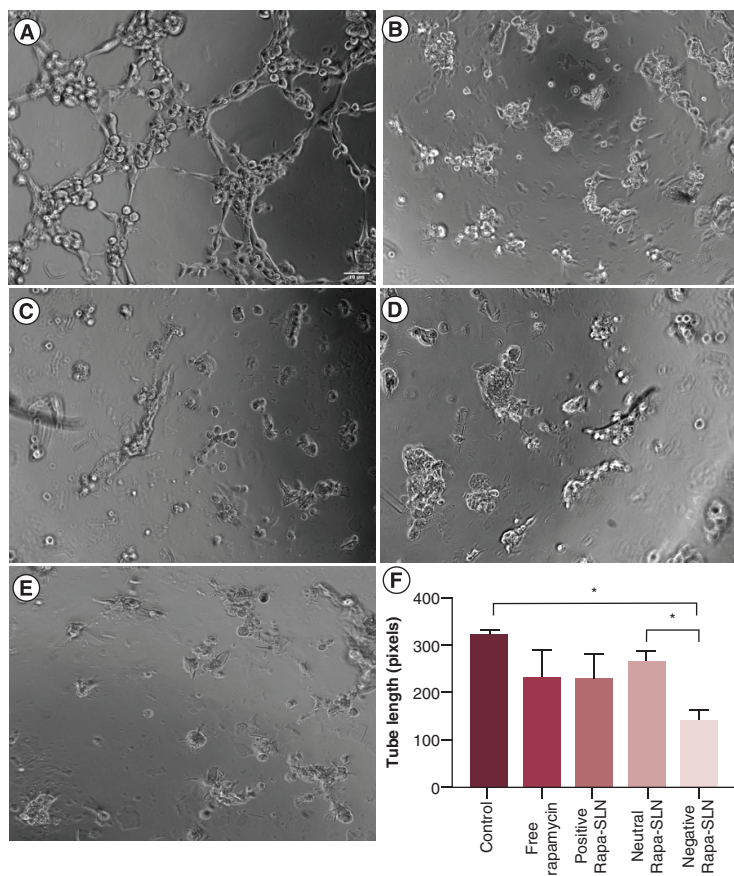


**Figure 7. Tube formation assay of human lymphatic endothelial cells.** Grown on matrigel for 6 h with (A) no treatment or treatment with 200 nM of (B) free rapamycin, (C) positive Rapa-SLNs, (D) neutral Rapa-SLNs, (E) negative Rapa-SLNs and (F) average tube length of tube formations in pixels following each treatment. Images evaluated using ImageJ software. Scale bar = 10  $\mu$ m. Data expressed as the mean of three independent measurements  $\pm$  SEM. \* $p < 0.05$  compared with control. Rapa-SLN: Rapamycin solid lipid nanoparticle.

### *Rapa-SLNs inhibit the enhanced tube formation of HLEC*

In addition to increased proliferation and growth of smooth like muscle cells in the lungs, LAM is also associated with increased lymphangiogenesis [2]. This is thought to be a result of the increased upregulation of the mTOR pathway in LAM, which increases the expression of VEGF receptor C and D (VEGFR) on the surface of LAM cells [73], causing increased formation of new lymphatic vessels. Rapamycin has been shown by multiple studies [74–76] to inhibit this process by binding to the FK506 subunit, associated with mTOR. Here, the tube formation assay was used to assess the ability of the differently charged Rapa-SLN formulations to inhibit lymphangiogenesis in HLECs, compared with untreated controls and free rapamycin.

Figure 7A shows that the untreated control cells of HLEC grown on matrigel for 6 h form a branching mesh work of tube-like capillary structures concurrent with reports in the literature [29,77–79]. Treatment with 200 nM of free rapamycin in Figure 7B shows shorter clump-like unstructured capillary structures that are disconnected from one another, while treatment with neutral (Figure 7D) and positively (Figure 7C) charged Rapa-SLNs resulted in similar structures. While negatively charged Rapa-SLNs resulted in similar disorganized structures, the clumps of tube structures appear shorter and further apart, compared with treatment with free rapamycin and the other charged Rapa-SLNs (Figure 7E). This is further confirmed by analysis of the tube length of the capillary structures following the different treatments (Figure 7F), where the negatively charged Rapa-SLNs resulted in a significantly shorter tube length compared with the untreated control and neutral Rapa-SLNs. However, analysis and quantification of the tube length demonstrated that there was only a significant difference in tube length after treatment with free rapamycin and positive Rapa-SLNs compared with untreated control cells. These quantitative and qualitative results imply that negative Rapa-SLNs can result in more effective inhibition of lymphangiogenesis in HLECs. These results could be attributed to the higher permeability of negative Rapa-SLNs through the endothelial cells compared with free rapamycin, neutral and positively charged Rapa-SLNs, as shown in the *in vitro* transport

study. This would allow the negatively charged Rapa-SLNs to enter the cells faster, releasing the rapamycin more effectively and allowing it to have an inhibitory effect on tube formation.

## Conclusion

This second part of a two-part study investigated and characterized the effects of surface charge of Rapa-SLNs on its ability to access the lymphatic system once inhaled. The formulations were first characterized for their *in vitro* release profiles and penetration through the bronchial endothelium, in comparison to free rapamycin. Results showed that all three Rapa-SLNs of the same size, regardless of charge, had a more sustained release compared with free rapamycin, while the positive and negative Rapa-SLNs showing the fastest rate of transport across the bronchial epithelium. The negative Rapa-SLNs showed the least accumulation of particles inside the cells after the transport study, indicating a more efficient *trans*-epithelial transport compared with the positive Rapa-SLNs. Furthermore, *in vitro* HLEC studies showed that negative Rapa-SLNs presented a higher permeability through the lymphatic endothelium, compared with the other SLNs and free rapamycin. Negative Rapa-SLNs were also found to be the less toxic compared with the positive Rapa-SLNs. Additionally, while all three Rapa-SLNs resulted in a decrease in tube formation compared with the untreated control, negative Rapa-SLNs showed a significant reduction in the tube formation length compared with the control. In contrast, both negative and positively charge Rapa-SLNs were able to inhibit the enhanced proliferation of MEF cells to a greater extent compared with neutral Rapa-SLNs.

In summary, surface-charged Rapa-SLNs seem to be more favorable in terms of its ability to provide a more sustained release profile of rapamycin *in vitro*, and ensuring efficient transport across the bronchial endothelium. Similarly, a positive and negative surface charge had an equally inhibitory effect on the enhanced proliferation of MEF cells. However, a negative surface charge may overall be the most favorable for treating LAM, as it allows the most efficient transport into the lymphatic endothelium and decrease in tube formation of the endothelial vessels in combination with its reduced toxicity to non-MEF cells. This would greatly improve the treatment of LAM, as the Rapa-SLNs could access extra pulmonary LAM cells in other organs more rapidly, while simultaneously reducing the amount of lymphangiogenesis and hence the spreading of LAM cells. Future *in vivo* studies will need to further verify these results, by investigation the biodistribution, safety profile and pharmacokinetics of the Rapa-SLN formulations.

In conclusion, rapamycin delivered via the pulmonary route using SLNs approximately 200 nm and a negative surface charge, could potentially be a promising alternative treatment to the current oral treatment for LAM.

## Summary points

- Three rapamycin solid lipid nanoparticle (Rapa-SLN) formulations with different surface charges were generated using a hot evaporation technique and addition of surface-modifying additives.
- Rapamycin encapsulated in lipid carrier displayed more sustained release profiles *in vitro* compared with free rapamycin.
- Charged Rapa-SLNs (positive and negative) were equally potent at inhibiting the enhanced proliferation displayed by a cellular model of lymphangioleiomyomatosis using negative tuberous sclerosis complex-2 mice embryonic fibroblast cells compared with neutral Rapa-SLN and free rapamycin.
- Negatively and positively charged Rapa-SLNs showed the most efficient transport across the bronchial epithelium.
- Negatively charged Rapa-SLNs were less toxic toward human lymphatic endothelial cells compared with positive and neutral Rapa-SLNs as well as free rapamycin.
- Negative Rapa-SLNs had the highest permeability and transport rate across the lymphatic endothelium and was able to inhibit tube formation of lymphatic cells significantly, compared with untreated cells and other SLN formulation.

## Acknowledgments

The authors thank David Kwiatkowski and Vera Krymskaya for supplying the MEF cells.

## Financial & competing interests disclosure

The authors have no relevant affiliations or financial involvement with any organization or entity with a financial interest in or financial conflict with the subject matter or materials discussed in the manuscript. This includes employment, consultancies, honoraria, stock ownership or options, expert testimony, grants or patents received or pending, or royalties.

No writing assistance was utilized in the production of this manuscript.

## References

Papers of special note have been highlighted as: ●● of considerable interest

- 1 Sarbassov DD, Ali SM, Kim DH *et al.* Rictor, a novel binding partner of mTOR, defines a rapamycin-insensitive and raptor-independent pathway that regulates the cytoskeleton. *Curr. Biol.* 14(14), 1296–1302 (2004).
- 2 Kumasaka T, Seyama K, Mitani K *et al.* Lymphangiogenesis-mediated shedding of LAM cell clusters as a mechanism for dissemination in lymphangioliomyomatosis. *Am. J. Surg. Pathol.* 29(10), 1356–1366 (2005).
- **It highlights how the spreading of lymphangioliomyomatosis cells occurs via the lymphatic system.**
- 3 Harknett EC, Chang WY, Byrnes S *et al.* Use of variability in national and regional data to estimate the prevalence of lymphangioliomyomatosis. *QJM* 104(11), 971–979 (2011).
- 4 Ferrans VJ, Yu ZX, Nelson WK *et al.* Lymphangioliomyomatosis (LAM): a review of clinical and morphological features. *J. Nippon Med. Sch.* 67(5), 311–329 (2000).
- 5 Cohen MM, Pollock-Barziv S, Johnson SR. Emerging clinical picture of lymphangioliomyomatosis. *Thorax* 60(10), 875–879 (2005).
- 6 Zheng J, Sambol NC, Zimmerman DJ, Zaidi A. Population pharmacokinetics (PK) of sirolimus. *Clin. Pharmacol. Ther.* 59(2), 150–150 (1996).
- 7 Bissler JJ, McCormack FX, Young LR *et al.* Sirolimus for angiomyolipoma in tuberous sclerosis complex or lymphangioliomyomatosis. *N. Engl. J. Med.* 358(2), 140–151 (2008).
- 8 Desai N, Heenan S, Mortimer PS. Sirolimus-associated lymphoedema: eight new cases and a proposed mechanism. *Br. J. Dermatol.* 160(6), 1322–1326 (2009).
- 9 Landh E, Moir LM, Gomes Dos Reis L, Traini D, Young PM, Ong HX. Inhaled rapamycin solid lipid nano particles for the treatment of Lymphangioliomyomatosis. *Eur. J. Pharm. Sci.* 142, 105098 (2019).
- 10 Labiris NR, Dolovich MB. Pulmonary drug delivery. Part I: physiological factors affecting therapeutic effectiveness of aerosolized medications. *Br. J. Clin. Pharmacol.* 56(6), 588–599 (2003).
- 11 Stump B, Cui Y, Kidambi P, Lamattina AM, El-Chemaly S. Lymphatic changes in respiratory diseases: more than just remodeling of the lung? *Am. J. Respir. Cell Mol. Biol.* 57(3), 272–279 (2017).
- 12 Li AV, Moon JJ, Abraham W *et al.* Generation of effector memory T cell-based mucosal and systemic immunity with pulmonary nanoparticle vaccination. *Sci. Transl. Med.* 5(204), 204ra130 (2013).
- 13 Videira MA, Botelho MF, Santos AC, Gouveia LF, De Lima JJ, Almeida AJ. Lymphatic uptake of pulmonary delivered radiolabelled solid lipid nanoparticles. *J. Drug Target.* 10(8), 607–613 (2002).
- 14 Latimer P, Menchaca M, Snyder RM *et al.* Aerosol delivery of liposomal formulated paclitaxel and vitamin E analog reduces murine mammary tumor burden and metastases. *Exp. Biol. Med. (Maywood)* 234(10), 1244–1252 (2009).
- 15 Trevaskis NL, Kaminskas LM, Porter CJ. From sewer to saviour – targeting the lymphatic system to promote drug exposure and activity. *Nat. Rev. Drug Discov.* 14(11), 781–803 (2015).
- 16 Mohammad AK, Amayreh LK, Mazzara JM, Reineke JJ. Rapid lymph accumulation of polystyrene nanoparticles following pulmonary administration. *Pharm. Res.* 30(2), 424–434 (2013).
- 17 Kaur CD, Nahar M, Jain NK. Lymphatic targeting of zidovudine using surface-engineered liposomes. *J. Drug Target.* 16(10), 798–805 (2008).
- 18 Patel HM, Boodle KM, Vaughan-Jones R. Assessment of the potential uses of liposomes for lymphoscintigraphy and lymphatic drug delivery. Failure of 99m-technetium marker to represent intact liposomes in lymph nodes. *Biochim. Biophys. Acta* 801(1), 76–86 (1984).
- **In vivo study in rats showing that negatively charged liposomes result in increased lymph node retention compared with positively and neutrally charged liposomes, 4 h after delivery.**
- 19 Rao DA, Forrest ML, Alani AW, Kwon GS, Robinson JR. Biodegradable PLGA based nanoparticles for sustained regional lymphatic drug delivery. *J. Pharm. Sci.* 99(4), 2018–2031 (2010).
- 20 Kaminskas LM, Kota J, McLeod VM, Kelly BD, Karellas P, Porter CJ. PEGylation of polylysine dendrimers improves absorption and lymphatic targeting following SC administration in rats. *J. Control. Rel.* 140(2), 108–116 (2009).
- 21 Li SD, Huang L. Pharmacokinetics and biodistribution of nanoparticles. *Mol. Pharm.* 5(4), 496–504 (2008).
- 22 Yu B, Zhang Y, Zheng W, Fan C, Chen T. Positive surface charge enhances selective cellular uptake and anticancer efficacy of selenium nanoparticles. *Inorg. Chem.* 51(16), 8956–8963 (2012).
- 23 Salvioni L, Galbiati E, Collico V *et al.* Negatively charged silver nanoparticles with potent antibacterial activity and reduced toxicity for pharmaceutical preparations. *Int. J. Nanomedicine* 12, 2517–2530 (2017).
- 24 Landh E, Moir LM, Bradbury P, Traini D, Young PM, Ong HX. Properties of rapamycin solid lipid nanoparticles for lymphatic access through the lungs: part I: the effect of nanoparticle size. *Nanomedicine (Lond.)* doi:10.2217/nmm-2020-0077 (2020) (In Press).
- 25 Platel A, Carpentier R, Becart E, Mordacq G, Betbeder D, Nessler F. Influence of the surface charge of PLGA nanoparticles on their *in vitro* genotoxicity, cytotoxicity, ROS production and endocytosis. *J. Appl. Toxicol.* 36(3), 434–444 (2016).

- 26 Wang R, Xiao R, Zeng Z, Xu L, Wang J. Application of poly(ethylene glycol)-distearoylphosphatidylethanolamine (PEG-DSPE) block copolymers and their derivatives as nanomaterials in drug delivery. *Int. J. Nanomedicine* 7, 4185–4198 (2012).
- 27 Haghi M, Young PM, Traini D, Jaiswal R, Gong J, Bebawy M. Time- and passage-dependent characteristics of a Calu-3 respiratory epithelial cell model. *Drug Dev. Ind. Pharm.* 36(10), 1207–1214 (2010).
- 28 FDA. Reviewer guidance for nebulizers, metered dose inhalers, spacers and actuators (1993). [www.fda.gov/cdrh/ode/784.pdf](http://www.fda.gov/cdrh/ode/784.pdf)
- 29 Luo Y, Liu L, Rogers D *et al.* Rapamycin inhibits lymphatic endothelial cell tube formation by downregulating vascular endothelial growth factor receptor 3 protein expression. *Neoplasia* 14(3), 228–237 (2012).
- 30 Schacht V, Ramirez MI, Hong YK *et al.* T1alpha/podoplanin deficiency disrupts normal lymphatic vasculature formation and causes lymphedema. *EMBO J.* 22(14), 3546–3556 (2003).
- 31 Souto EB, Mehnert W, Müller RH. Polymorphic behaviour of Compritol 888 ATO as bulk lipid and as SLN and NLC. *J. Microencapsul.* 23(4), 417–433 (2006).
- 32 Aburahma MH, Badr-Eldin SM. Compritol 888 ATO: a multifunctional lipid excipient in drug delivery systems and nanopharmaceuticals. *Expert Opin. Drug Deliv.* 11(12), 1865–1883 (2014).
- 33 Khan AA, Abdulbaqi IM, Abou Assi R, Murugaiyah V, Darwis Y. Lyophilized hybrid nanostructured lipid carriers to enhance the cellular uptake of verapamil: statistical optimization and *in vitro* evaluation. *Nanoscale Res. Lett.* 13(1), 323 (2018).
- 34 Shi L, Li Z, Yu L, Jia H, Zheng L. Effects of surfactants and lipids on the preparation of solid lipid nanoparticles using double emulsion method. *J. Dispers. Sci. Technol.* 32(2), 254–259 (2011).
- 35 Irannejad H. Nitrogen rich heterocycles as a privileged fragment in lead discovery. *Med. Anal. Chem. Int. J.* 2(3), 1–6 (2018).
- 36 Singh I, Swami R, Khan W, Sistla R. Lymphatic system: a prospective area for advanced targeting of particulate drug carriers. *Expert Opin. Drug Deliv.* 11(2), 211–229 (2014).
- 37 Lee SY, Kim SJ. Dehydration behaviour of hexadecyltrimethylammonium-exchanged smectite. *Clay Miner.* 38(2), 225–232 (2002).
- 38 Ramimoghdam D, Hussein MZ, Taufiq-Yap YH. The effect of sodium dodecyl sulfate (SDS) and cetyltrimethylammonium bromide (CTAB) on the Properties of ZnO synthesized by hydrothermal method. *Int. J. Mol. Sci.* 13(10), 13275–13293 (2012).
- 39 Nukala RK, Boyapally H, Slipper IJ, Mendham AP, Douroum D. The application of electrostatic dry powder deposition technology to coat drug-eluting stents. *Pharm. Res.* 27(1), 72–81 (2010).
- 40 Emami S, Valizadeh H, Islambulchilar Z, Zakeri-Milani P. Development and physicochemical characterization of sirolimus solid dispersions prepared by solvent evaporation method. *Adv. Pharm. Bull.* 4(4), 369–374 (2014).
- 41 Moore JW, Flanner HH. Mathematical comparison of dissolution profiles. *Pharm. Technol.* 20(6), 64–74 (1996).
- 42 Silva A, Martins-Gomes C, Coutinho Te *et al.* Soft cationic nanoparticles for drug delivery: production and cytotoxicity of solid lipid nanoparticles (SLNs). *Appl. Sci.* 9(20), 4438 (2019).
- 43 Budhian A, Siegel SJ, Winey KI. Production of haloperidol-loaded PLGA nanoparticles for extended controlled drug release of haloperidol. *J. Microencapsul.* 22(7), 773–785 (2005).
- 44 Gref R, Luck M, Quellec P *et al.* ‘Stealth’ corona-core nanoparticles surface modified by polyethylene glycol (PEG): influences of the corona (PEG chain length and surface density) and of the core composition on phagocytic uptake and plasma protein adsorption. *Colloids Surf. B Biointerfaces* 18(3–4), 301–313 (2000).
- 45 Sathyamoorthy N, Magharla DD, Vankayalu SD. Effect of surface modification on the *in vitro* protein adsorption and cell cytotoxicity of vinorelbine nanoparticles. *J. Pharm. Bioallied Sci.* 9(2), 135–143 (2017).
- 46 Stewart CE, Torr EE, Mohd Jamili NH, Bosquillon C, Sayers I. Evaluation of differentiated human bronchial epithelial cell culture systems for asthma research. *J. Allergy (Cairo)* 2012, 943982 (2012).
- 47 Bur M, Huwer H, Muys L, Lehr CM. Drug transport across pulmonary epithelial cell monolayers: effects of particle size, apical liquid volume, and deposition technique. *J. Aerosol Med. Pulm. Drug Deliv.* 23(3), 119–127 (2010).
- 48 Ong HX, Traini D, Young PM. Pharmaceutical applications of the Calu-3 lung epithelia cell line. *Expert Opin. Drug Deliv.* 10(9), 1287–1302 (2013).
- 49 Olsson B, Bondesson E, Borgström L *et al.* Pulmonary drug metabolism, clearance and absorption. In: *Controlled Pulmonary Drug Delivery*. Springer Science NY, USA 21–50 (2011).
- 50 Bannunah AM, Vllasaliu D, Lord J, Stolnik S. Mechanisms of nanoparticle internalization and transport across an intestinal epithelial cell model: effect of size and surface charge. *Mol. Pharm.* 11(12), 4363–4373 (2014).
- 51 Rojanasakul Y, Wang LY, Bhat M, Glover DD, Malanga CJ, Ma JK. The transport barrier of epithelia: a comparative study on membrane permeability and charge selectivity in the rabbit. *Pharm. Res.* 9(8), 1029–1034 (1992).
- 52 Harush-Frenkel O, Rozentur E, Benita S, Altschuler Y. Surface charge of nanoparticles determines their endocytic and transcytotic pathway in polarized MDCK cells. *Biomacromolecules* 9(2), 435–443 (2008).
- 53 Bannunah AM, Vllasaliu D, Lord J, Stolnik S. Mechanisms of nanoparticle internalization and transport across an intestinal epithelial cell model: effect of size and surface charge. *Mol. Pharm.* 11(12), 4363–4373 (2014).

- 54 Dausend J, Musyanovych A, Dass M *et al.* Uptake mechanism of oppositely charged fluorescent nanoparticles in HeLa cells. *Macromol. Biosci.* 8(12), 1135–1143 (2008).
- 55 Goncharova EA, Goncharov DA, Eszterhas A *et al.* Tuberin regulates p70 S6 kinase activation and ribosomal protein S6 phosphorylation. A role for the TSC2 tumor suppressor gene in pulmonary lymphangioleiomyomatosis (LAM). *J. Biol. Chem.* 277(34), 30958–30967 (2002).
- 56 Ng HY, Oliver BG, Burgess JK, Krymskaya VP, Black JL, Moir LM. Doxycycline reduces the migration of tuberous sclerosis complex-2 null cells – effects on RhoA-GTPase and focal adhesion kinase. *J. Cell. Mol. Med.* 19(11), 2633–2646 (2015).
- ***In vitro* cell study providing evidence that rapamycin significantly inhibits proliferation in a lymphangioleiomyomatosis model of tuberous sclerosis complex-2-negative mice embryonic fibroblast cells.**
- 57 Bernfield M, Götte M, Park PW *et al.* Functions of cell surface heparan sulfate proteoglycans. *Annu. Rev. Biochem.* 68, 729–777 (1999).
- 58 Zhao J, Stenzel MH. Entry of nanoparticles into cells: the importance of nanoparticle properties. *Polym. Chem.* 9(3), 259–272 (2018).
- 59 Thorek DL, Tsourkas A. Size, charge and concentration dependent uptake of iron oxide particles by nonphagocytic cells. *Biomaterials* 29(26), 3583–3590 (2008).
- 60 Slowing I, Trewyn BG, Lin VS. Effect of surface functionalization of MCM-41-type mesoporous silica nanoparticles on the endocytosis by human cancer cells. *J. Am. Chem. Soc.* 128(46), 14792–14793 (2006).
- 61 Khine YY, Callari M, Lu H, Stenzel MH. Direct correlation between zeta potential and cellular uptake of poly(methacrylic acid) post-modified with guanidinium functionalities. *Macromol. Chem. Phys.* 217(20), 2302–2309 (2016).
- 62 Cho EC, Xie J, Wurm PA, Xia Y. Understanding the role of surface charges in cellular adsorption versus internalization by selectively removing gold nanoparticles on the cell surface with a I2/KI etchant. *Nano Lett.* 9(3), 1080–1084 (2009).
- 63 Li S, Malmstadt N. Deformation and poration of lipid bilayer membranes by cationic nanoparticles. *Soft Matter* 9(20), 4969–4976 (2013).
- 64 Takakura Y, Atsumi R, Hashida M, Sezaki H. Development of a novel polymeric prodrug of mitomycin C, mitomycin C-dextran conjugate with anionic charge. II. Disposition and pharmacokinetics following intravenous and intramuscular administration. *Int. J. Pharm.* 37(1), 145–154 (1987).
- 65 Triacca V, Guc E, Kilarski WW, Pisano M, Swartz MA. Transcellular pathways in lymphatic endothelial cells regulate changes in solute transport by fluid stress. *Circ. Res.* 120(9), 1440–1452 (2017).
- 66 Wiig H, Swartz MA. Interstitial fluid and lymph formation and transport: physiological regulation and roles in inflammation and cancer. *Physiol. Rev.* 92(3), 1005–1060 (2012).
- 67 Feng D, Nagy JA, Dvorak HF, Dvorak AM. Ultrastructural studies define soluble macromolecular, particulate, and cellular transendothelial cell pathways in venules, lymphatic vessels, and tumor-associated microvessels in man and animals. *Microsc. Res. Tech.* 57(5), 289–326 (2002).
- 68 Negrini D, Moriondo A. Lymphatic anatomy and biomechanics. *J. Physiol.* 589(12), 2927–2934 (2011).
- 69 Trzewik J, Mallipattu SK, Artmann GM, Delano FA, Schmid-Schönbein GW. Evidence for a second valve system in lymphatics: endothelial microvalves. *FASEB J.* 15(10), 1711–1717 (2001).
- 70 Zhang LW, Monteiro-Riviere NA. Mechanisms of quantum dot nanoparticle cellular uptake. *Toxicol. Sci.* 110(1), 138–155 (2009).
- 71 Sahay G, Kim JO, Kabanov AV, Bronich TK. The exploitation of differential endocytic pathways in normal and tumor cells in the selective targeting of nanoparticulate chemotherapeutic agents. *Biomaterials* 31(5), 923–933 (2010).
- 72 Sahay G, Alakhova DY, Kabanov AV. Endocytosis of nanomedicines. *J. Control. Rel.* 145(3), 182–195 (2010).
- 73 Kumasaka T, Seyama K, Mitani K *et al.* Lymphangiogenesis in lymphangioleiomyomatosis: its implication in the progression of lymphangioleiomyomatosis. *Am. J. Surg. Pathol.* 28(8), 1007–1016 (2004).
- 74 Huber S, Bruns CJ, Schmid G *et al.* Inhibition of the mammalian target of rapamycin impedes lymphangiogenesis. *Kidney Int.* 71(8), 771–777 (2007).
- 75 Kobayashi S, Kishimoto T, Kamata S, Otsuka M, Miyazaki M, Ishikura H. Rapamycin, a specific inhibitor of the mammalian target of rapamycin, suppresses lymphangiogenesis and lymphatic metastasis. *Cancer Sci.* 98(5), 726–733 (2007).
- 76 Hammer T, Tritsaris K, Hubschmann MV *et al.* IL-20 activates human lymphatic endothelial cells causing cell signalling and tube formation. *Microvasc. Res.* 78(1), 25–32 (2009).
- 77 Wen J, Fu AF, Chen LJ *et al.* Liposomal honokiol inhibits VEGF-D-induced lymphangiogenesis and metastasis in xenograft tumor model. *Int. J. Cancer* 124(11), 2709–2718 (2009).
- 78 Danussi C, Spessotto P, Petrucco A *et al.* Emilin1 deficiency causes structural and functional defects of lymphatic vasculature. *Mol. Cell. Biol.* 28(12), 4026–4039 (2008).
- 79 Podgrabinska S, Braun P, Velasco P, Kloos B, Pepper MS, Skobe M. Molecular characterization of lymphatic endothelial cells. *Proc. Natl. Acad. Sci. USA* 99(25), 16069–16074 (2002).